Journal of Manufacturing Processes 50 (2020) 192–203

Contents lists available at ScienceDirect

Journal of Manufacturing Processes

journal homepage: www.elsevier.com/locate/manpro

Numerical and experimental study of discharge mechanism in the electrochemical discharge machining process

S. Elhami, M.R. Razfar*

Department of Mechanical Engineering, Amirkabir University of Technology, 424, Hafez Ave, Tehran, Iran

ARTICLE INFO

Keywords:
Discharge simulation
Electro-chemical discharge machining
Material removal

ABSTRACT

Electrochemical discharge machining (ECDM) is a modern machining process which can be applied to the special materials with unique properties. Glass and ceramics are major applications of the mentioned process. ECDM includes variant mechanisms of material removal (MR) in which discharge (thermal) mechanism plays the most important role in comparison to other mechanisms. This research introduces a new approach to simulate the discharge phenomenon and the consequent volume of removed material. Despite previous researches which implemented a simple thermal simulation based on Gaussian distribution, the current model considers different constitutive phenomena of discharge (plasma) and presents a more realistic numerical model. Electric current, electromagnetic field, and heat transfer are major effective phenomena on the plasma behavior which are considered in simulations and evaluated simultaneously, for all components of ECDM configuration. Special experiments are designed to validate the predictions of the model. The single discharge mode of the ECDM process is applied and two main parameters of hole diameter and MR are measured to compare with computed results. Consecutive actual images and current signal diagrams determined 37 V as a critical voltage to appear the discharge phenomenon. Results showed that the developed model has errors of 14.33 % and 31.52 % in the prediction of hole diameter and MR, respectively.

1. Introduction

Electro-chemical discharge machining is a nontraditional machining process which can be applied to shape nonconductive materials such as glasses and ceramics. This process includes different physical and chemical phenomena such as electrical discharge and chemical etching.

Each phenomenon effects on the material removal (MR) of the ECDM process but some of them have great influence. Between variant phenomena, electrical discharge plays an important role in the MR of the ECDM process. Sarkar et al. studied the discharge phenomenon during the ECDM process and observed small spherical particles which show the rapid solidification of molten materials. They concluded that every discharge transfers significant thermal energy to a small area on the workpiece and melt (or vaporize) a small quantity of workpiece material [1]. On the other hand, the applicable electrolyte as an active chemical material causes a chemical reaction between components. A very smooth surface of the workpiece after material removal shows the effect of a chemical reaction. Hence, chemical etching as another mechanism of MR has a small contribution to the total MR. A chemical reaction is very slow so the evaluation of MR caused by electrical discharge can lead to achieve the total MR as an important characteristic of the ECDM process.

1.1. Discharge description

The expression of electrical discharge employs whenever a current is forced to pass through the specific space. In another word, the plasma channel constitutes the electric discharge and every electric discharge associated with the formation of a plasma channel in a nonconductive environment.

Francis et al. defined the plasma as a semi-neutral gas, includes neutral and charged particles, which presents a collective behavior. He classified three general approaches to model the plasma behavior as follows [2]:

1 Kinetic: In this method, the distribution and behavior of every single particle (such as dissociation, ionization, excitation and …) are considered and applied in the simulation. Hence significant computation time is required.
2 Fluid: In this procedure, plasma is supposed as a uniform fluid with macroscopic specifications. This method is more efficient and can be implemented to simulate more complex types of plasma.

* Corresponding author.
E-mail address: Razfar@aut.ac.ir (M.R. Razfar).

https://doi.org/10.1016/j.jmapro.2019.12.040
Received 11 September 2019; Received in revised form 27 October 2019; Accepted 20 December 2019
Available online 26 December 2019

3 Combined Approach: In this approach, the positive column as the main part of plasma assumes to behave as a fluid. On the other hand, the kinetic approach is considered for regions close to the electrodes which are known as cathodic and anodic regions.

For the present research, particle colliding details such as chemical relations, the quantity of transferred energy and resulted particles are not known, clearly. Furthermore, Francis et al. studied other types of plasma which exist in nature and laboratory condition and stated that about 80 % of all types of plasma can be modeled using fluid assumption [2]. Hence, the application of a fluidic approach can achieve trustable results to simulate the plasma (discharge) phenomenon during the ECDM process.

1.2. Discharge type and LTE

Generally, there are three types of Townsend, Glow and Arc discharges in a gas environment.

I–V diagram is a unique tool which presents specific results in every machining condition and presents the variations of Ampere (I) and Voltage (V) as two main factors of discharge in the electrical circuit of the ECDM process. Wuthrich et al. employed the mentioned relation and classified different discharges according to the I–V diagram (Fig. 1-a) [3]. According to Fig. 1-a, Arc discharge takes place in high pressure (between 0.5–100 bar), low voltage (between 10–50 V) and high current (1–100 A) which are in agreement with discharge properties of the ECDM process [3].

According to a comprehensive study, Fridman et al. determined the temperature as the most important parameter which has a close relation to the energy of the particle [4]. Energy is an important parameter because it is converted to heat in the surfaces of electrodes and determines the material removal rate. Due to different types of particles involved in plasma composition, plasma as a multi-particle system can present different temperatures.

Max et al. stated if proper time, energy, and high density of electrons are available, all particles (positive and negative ions and neutral particles) will be in the Local Temperature Equilibrium (LTE) [5]. In this state, every point of plasma is specified with a single temperature (instead of consideration different temperatures for different particles) and plasma can be supposed to behave as a fluid. Now, there is a basic question about the governing LTE condition in Arc discharge of the ECDM process. Fig. 1-b shows the temperature of particles during high and low-pressure Arc discharges which clearly presents the dependency of LTE condition to the Arc pressure. In this regard, the ECDM process in which the pressure of hydrogen gas is equal to the atmospheric pressure finds the condition of high-pressure Arc. As can be seen, in the pressure of one bar, all particles have the same temperature and LTE conditions can be considered to simulate the Arc discharge of the ECDM process.

1.3. Literature review

Many researchers have attempted to simulate the ECDM process but they used a simple thermal model which implements Gaussian thermal distribution. This method pays attention only to the thermal distribution on the workpiece and does not consider changes in other components.

As a pioneer in the simulation of the ECDM process, Jain et al. used a FEM method to estimate the volume of removed material. The presented numerical model included a square section plasma channel. Results of temperature distribution on the workpiece showed that the presented model predicted a little larger values of MR in comparison to experiments [6]. Many computational simplifications were considered and the assumption of plasma with square section was far from the real condition. They were pioneers of the Gaussian distribution base simulation of the ECDM process and experimentally, formulated the input energy which widely used in the next investigations.

Bhondwe et al. employed Gaussian thermal distribution to simulate MR during the ECDM process considering Al_2O_3 ceramic and glass as workpieces. Considering the specific condition of this research, they presented an experimental equation to relate electrolyte concentration to the charactristics of Gaussian distribution [7]. Basically, this research used the same procedure close to pioneers and only considered a workpiece and did not pay attention to other components.

Wei et al. simulated the ECDM process in a single discharge mode using ANSYS software. They used the Fascio statistical method to determine the discharge frequency and totally, the evaluation of machining depth. Experimental verification of machining depth showed a good agreement with numerical results except at the beginning of the machining process [8]. Fascio method based on a statistical approach which was used to extract the specifications of single discharge from a multi-discharge state but due to the statistical nature, it is not accurate in general applications. Also, the FEM section of simulation included a common thermal model included Gaussian distribution. Also, boundary conditions were the same in the mentioned researches.

Jiang et al. studied the energy of discharges during the ECDM process. In this regard, they used tools with cylindrical and conical shapes. The electrical field modeling in the environment of COMSOL showed that the tip of the conical tool and circle of the cylindrical tool end are the most possible locations to initiate the discharge. Their results were matched to experimental observations [9]. Also, Jiang et al. developed a theoretical model to predict the thickness of gas film based

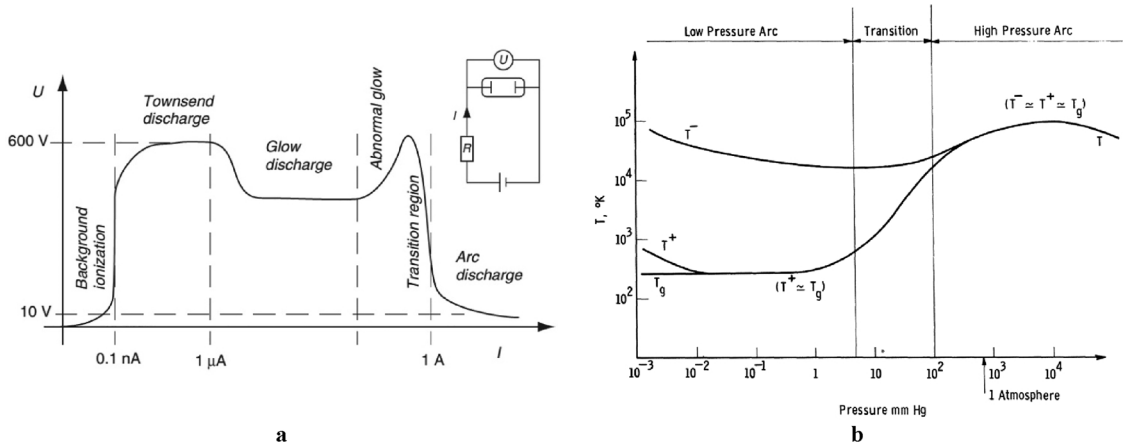

Fig. 1. a) I–V diagram used by Wuthrich et al. to determine discharge characteristics [3] b) Results of Max et al. research to determine the temperature of particles versus time in the case of Arc discharge [5].

on the theory of electrolysis phenomenon. They verified the theoretical model with experiments and stated the mean thickness of the gas film in the range of 17–29 μm [10]. However, in the next research, larger values of the thickness of gas film are achieved. Gaussian thermal distribution was repeated in this research in the same manner as previous investigations. Results of electrical field modeling were not used in thermal modeling and only presented in a separate section of research.

Kamaraj et al. presented a theoretical model to predict the temperature distribution on the workpiece during electrochemical discharge drilling. Their model was based on a half-sphere assumption of the volume of removed material by a single discharge so it was applicable only in low depth holes. The model had a prediction error of 15 % compared to experimental results [11]. The half-square shape of the MR area rarely happens in the real condition so achieved results are useful in a very specific condition. MR is the main output of the ECDM process so presented simulations should pay attention to this important output but this research did not continue computation on the main outputs of the ECDM process and only attempt to predict temperature distribution.

Goud et al. developed a 3D model to predict the volume of removed material during the single mode of the ECDM process. They studied the effect of electrolyte concentration and observed that a higher concentration resulted in more removed material [12]. However, this research included the innovation of 3D simulation instead of 2D modeling but this research applied a familiar trend to simulate discharge using a thermal model based on Gaussian thermal distribution. Due to the geometrical dimension of holes during the ECDM process and considering the cost and time of computation, it seems 2D geometry can achieve better efficiency.

Bhondwe et al. presented a model with a prediction error of 40 % for MR. Kamaraj et al. only predicted entrance overcut with an error of 15 %. Goud et al. presented a 3D model and found a prediction error of 20 %. In the mentioned researches and other similar investigations, the simulation of the ECDM process included a simple thermal model which was applied to the workpiece and other physical phenomena including the tool, gas film, and hydrogen (as main constitutive of the gas film) are ignored. Hence, current research tries to employ a different method and consider most of the physical phenomena which effect on the discharge (plasma) during the ECDM process. In this regard and as the first step, the type of discharge should be determined. According to previous explanations, the environmental condition of the ECDM process necessitates the formation of high-pressure Arc discharge. It is clear that LTE condition governs hence electrons and heavy particles have approximately an equal temperature and plasma (discharge) can be supposed to treat the same as fluid. Totally, authors consider plasma (discharge) as a fluid in the simulation process to predict MR and characteristics of components during the ECDM process.

2. Simulation of (Arc) discharge

In this research, a different simulation method of discharge during the ECDM process is implemented which has great advantages compared to the previous common procedure. In order to clarify the differences, the two diagrams are presented in Figs. 2 and 3. Fig. 2 shows the old procedure while Fig. 3 presents the new simulation method of discharge. In the previous method, by the application of Gaussian distribution, only the thermal behavior of the workpiece was considered and there was no attempt to model real discharge (plasma) and involved components. In the current research, authors try to simulate plasma as the main part of the ECDM process to present a semi-realistic numerical model. In this regard, cathode, anode, electrolyte and hydrogen gas (gas film) are considered in the simulations. The developed model includes the main physical phenomena of plasma. In order to determine MR, the distribution of thermal energy and temperature in all components is evaluated. Finally, the results of the workpiece phase change clearly present the volume of the removed material.

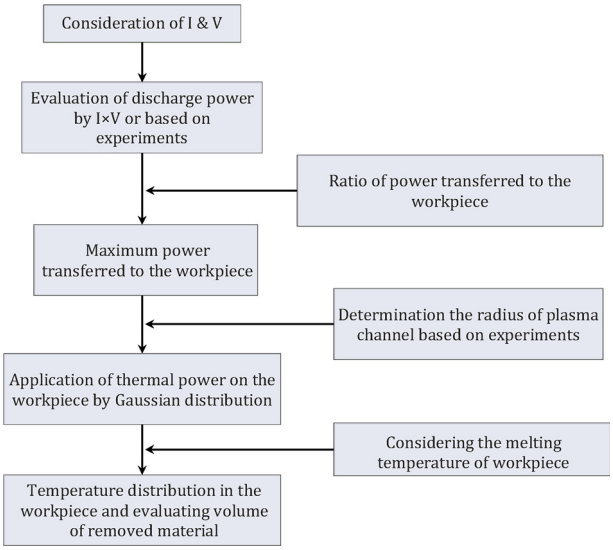

Fig. 2. Diagram of the ECDM simulation procedure in past researches.

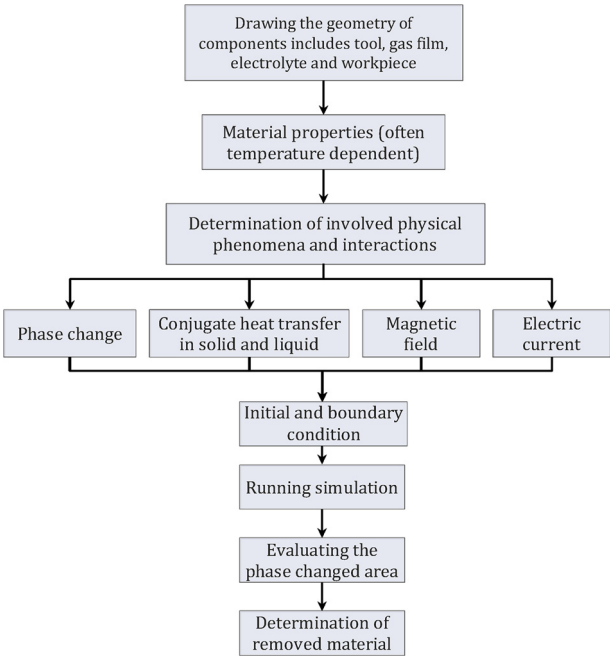

Fig. 3. Diagram of a new procedure of ECDM simulation.

One of the most important issues in the simulation of plasma is the temperature dependent properties of the main component. In this case, hydrogen is the main ingredient and Yos et al. has extracted related physical and mechanical properties which are applicable in the environment of COMSOL [13]. Also, temperature-dependent properties of other components including workpiece and tool is prepared in reference [14] and it is applicable to the simulation. Due to a lack of information, electrolyte properties were considered constant and independent of the temperature. The electric current as another input of simulation can be considered the same as a theoretical profile but in this research obtained from experiments (Section 3.1) to simulate a more realistic condition.

Also, all simulations are computed in the environment of COMSOL. This software has great potential to attribute different physical phenomena. Because of the multi-physic nature of the ECDM process, it seems that COMSOL provides the possibility to simulate the ECDM process in a more realistic manner.

2.1. Assumptions

The developed model contains simplifying assumptions as follows:

1 Numerical simulation limits to the positive column of plasma phenomena.
2 LTE condition is validated so plasma can be considered as a uniform fluid.
3 The effects of electrolyte (and workpiece) vaporized material on the plasma gas (hydrogen) are ignored.
4 The hydrogen gas which constitutes the plasma is considered homogenous.
5 Workpiece material assumes to be isotropic and homogenous.
6 Between different MR mechanisms in the ECDM process, only the thermal mechanism (by discharge) is considered.

2.2. Description of considered physical phenomena

Plasma nature includes different types of physical phenomena. Electric current, electromagnetic field, and heat transfer are major affective phenomena. Heat transfer is applied to two assortments of components including tool and workpiece as solid beside hydrogen gas film and electrolyte as liquid materials. In other words, conjugated heat transfer is implemented in simulations. Electric current and electromagnetic fields basically change the condition of hydrogen gas as the main position of plasma formation. Also, the phase change is considered for an electrolyte which converts from liquid to vapor and workpiece which changes from solid to liquid (electrolyte vapor and workpiece molten materials do not consider in simulations). Workpiece phase change determines the volume of removed materials. A major problem in plasma modeling is connecting different phenomena to each other. The multi-physic module of COMSOL provides an easier way to establish these connections. Multi-physics module includes:

- *The plasma heat source* simulates the thermal energy which is generated in the positive column of plasma. In the ECDM process, this area is filled with hydrogen gas. This sub-module relates electric and electromagnetic fields to the heat transfer physic and considers joule heating and radiation heat loss.
- *Boundary plasma heat source* is applied on the electrodes' surfaces and evaluates the effect of plasma on the anode and cathode surfaces.
- *The induction current density component* is applied to the constitutive gas of plasma (hydrogen gas) and evaluates the effects of electric and electromagnetic fields on the induced current in the positive column of plasma.

2.2.1. Plasma heat source

In this sub-module, the energy conservation equation is used which is as follows:

$$\rho C_p\left(\frac{\partial T}{\partial t} + u.\ \nabla T\right) - \nabla.\ (k\nabla T) = Q \tag{1}$$

which ρ is density, C_p and T are specific heat capacity and temperature, Q is a thermal source of plasma that mainly includes Joule heating. Joule heating is evaluated as follows:

$$Q = J.\ E, E = -\nabla V \tag{2}$$

J, E, and V are current density, electric field, and electric potential, respectively. In the mentioned type of plasma, the rule of constant electric current is established as follows:

$$\nabla.\ (-\sigma\nabla V + J_e) = 0 \tag{3}$$

in which, σ is the density of surface charges. In the direct current plasma, $J_e = 0$, hence this equation finds a simpler form.

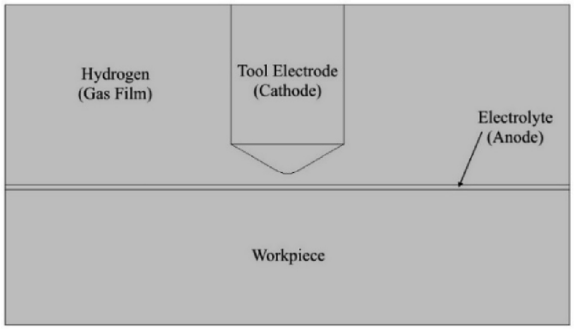

Fig. 4. Geometry of components in the simulation of the ECDM process.

2.2.2. Ion bombardment and thermionic emission on the cathode

On the effect of an electric field, positive ions are accelerated in the plasma channel toward the negative pole and collide to the cathode surface (ion bombardment) which results in heat generation. Colliding heavy particles to the cathode surface may lead emission of some of the electrons from the cathode surface which reduces the cathode temperature (secondary emission). The thermal flux, due to ion bombardment, is calculated as follows:

$$-\ n.\ (-k\nabla T) = -|J_{elec}|\ \phi_s + |J_{ion}|\ V_{ion} \tag{4}$$

where k is the thermal conductivity, ϕ_s, and V_{ion} are electrode work function (2.6 V) and ionization potential in the plasma (15.7 V). The ionic current density norm is as follows:

$$|J_{ion}| = |J.\ n| - |J_{elec}| \tag{5}$$

where $|J.\ n|$ is the current density in the normal direction. Also, the current density of electrons is stated as follows:

$$|J_{elec}| = \begin{cases} J_R(T),\ |J.\ n| > J_R(T) \\ |J.\ n|, |J.\ n| < J_R(T) \end{cases} \tag{6}$$

in this relation, $J_R(T)$ is Richardson-Dushman current density which is calculated by the following equation:

$$J_R(T) = A_R T^2 \exp\left(\frac{q\phi_{eff}}{k_B T}\right) \tag{7}$$

in which A_R is Richardson constant (120 A/(K*cm)^2), q and k_B are electric charges and Boltzmann constant. Also, ϕ_{eff} is the effective work function of the surface.

Eq. 6 determines the activation of secondary emission during plasma simulation. It means that if applied current density on the cathode is lower than $J_R(T)$, the secondary emission is not activated and if normal current density raises to values larger than $J_R(T)$, secondary emission (ion bombardment and thermionic emission) is activated. Eq. No. 6 states in case of a current density higher than $J_R(T)$, there are specific values for J_{elec} and J_{ion} and consequently the Eq. No. 4 is imported to calculations. But for a current density lower than $J_R(T)$, J_{ion} is equal to zero and consequently Eq. No. 4 is not considered in calculations.

2.2.3. Joule heating on the anode

In the plasma channel, electrons move toward the anode and collide to its surface and consequently generate heat energy. In a simplified condition, Kellogg et al. assumed ions do not collide to the anode surface [15]. Hence, the thermal flux on the anode surface is expressed as follows:

$$-\ n.\ (-k\nabla T) = |J.\ n|\ \phi_s \tag{8}$$

in which k and ϕ_s are thermal conductivity and the work function of anode surface, respectively.

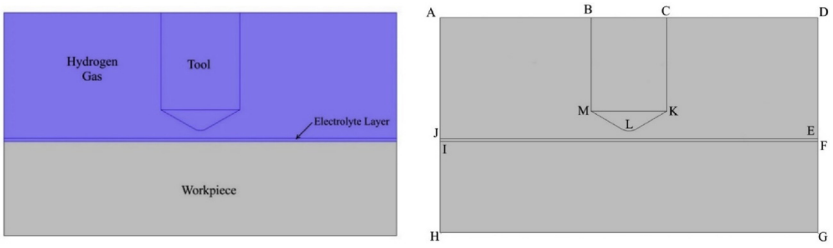

Fig. 5. a) Initial condition b) Different boundaries of considered geometry.

2.2.4. Heat transfer

In the COMSOL environment, heat transfer equation in solid is stated as follows:

$$\rho C_p\left(\frac{\partial T}{\partial t} + u_{trans}.\ \nabla T\right) + \nabla.\ (q + q_r) = -\alpha T:\ \frac{dS}{dt} + Q \tag{9}$$

On the left side of the equation, the first expression states the temperature variation versus time. The second expression shows thermodynamic coupling and the third expression states the thermal flux which is transferred from the control volume. On the right side, first and second expressions state surface tension and heat generation in the volume control, respectively. In this relation, q is conductive thermal flux, q_r is radiation heat flux, α is thermal expansion coefficient, S is stress matrix and u_{trans} is the velocity vector.

In the module of heat transfer in a fluid, the heat transfer general equation is expressed as follows:

$$\rho C_p\left(\frac{\partial T}{\partial t} + u.\ \nabla T\right) + \nabla.\ (q + q_r) = \alpha_p T\left(\frac{\partial p}{\partial t} + u.\ \nabla p\right) + \tau:\ \nabla u + Q \tag{10}$$

In the equation, α_p is the thermal expansion coefficient, τ is viscous stress matrix, p is pressure and Q is the heat generation source in the control volume.

2.2.5. Maxwell equations

Maxwell equations describe the creation of electric and electromagnetic fields in the effect of electric charges besides the interaction of mentioned fields on each other. In other words, Maxwell equations describe the behavior of electric charges and current as sources of electric and electromagnetic fields (two equations). Moreover, these equations explain how the variation of one field according to the time changes another field (two equations).

The first Maxwell equation is Gauss's law which states that the electric field has a direct relation to the number of related charges as follows:

$$\nabla.\ E = \frac{\rho}{\varepsilon_0} \tag{11}$$

In this relation, E, ρ, and ε_0 are an electric field, the density of electric charge and vacuum permittivity, respectively.

The second equation is Gauss's law for magnetism which states that single magnetic polar does not exist, so:

$$\nabla.\ B = 0 \tag{12}$$

where B is a magnetic field.

The third equation is known as Faraday's law of induction states that if magnetic field changes, an electric field induces in the circuit which is called induced electric field.

$$\nabla \times E = -\frac{\partial B}{\partial t} \tag{13}$$

The fourth equation which known as Ampère's circuital law states that a magnetic field can be produced in the effect of a variable electric field or electric current.

$$\nabla \times B = \mu_0 J + \mu_0 \varepsilon_0 \frac{\partial E}{\partial t} \tag{14}$$

in which, J and μ_0 are electric current density and vacuum permeability, respectively.

2.3. Geometry

According to the experimental configuration, considered components for the numerical model are the tool, workpiece, hydrogen gas, and a layer of electrolyte which are shown in Fig. 4. This geometry is acceptable when the formation of the gas film is completed so a layer of electrolyte is covered the workpiece. The thickness of the electrolyte layer was determined through primary experiments. Different values of voltage and different electrolyte thicknesses were considered and the closest value of thickness in experimental and simulation results was selected as the thickness of the electrolyte layer. During a single discharge of the ECDM process, the distance between the tool and workpiece is about 70 μm so in the model, this value is applied. Simulation time is determined by the electric current profile (Section 3.1) and considered about 15 μs.

2.4. Initial and boundary conditions

In this research, electrolysis as an initial step of the ECDM process is not considered in the simulation procedure. On the other hand, Kellogg et al. showed that electrolysis effects on the electrolyte temperature before the discharge occurs [15]. The initial temperature of the electrolyte can effect on the discharge behavior. So, Garbarz et al. in an experimental procedure determined 100 °C as the temperature of the electrolyte after electrolysis [16] and this value is employed as the initial temperature of electrolyte in discharge simulations. Due to the large contact area of gas film and electrolyte, the initial temperature of hydrogen around the tool is considered the same as an electrolyte (regions with blue color in Fig. 5-a).

Convection heat transfer occurs through JAB and CDE boundaries (Fig. 5-b) to the remained hydrogen of gas film. Heath et al. studied the convection heat transfer through a hydrogen environment which had characteristics close to the current research [17]. They achieved 3 W/(m^2 K) as the coefficient of convection heat transfer. The same value is employed in JAB and CDE boundaries. Boundaries of HI and FG have natural heat transfer through vertical walls. The workpiece in the GH boundary has natural convention through horizontal walls. Mentioned boundaries of the workpiece are in contact with electrolyte so for evaluation of natural convection and in order to simplify the calculation, water can be considered instead of actual electrolyte. The tool in BC boundary has conduction heat transfer to another part of the tool. CKLMB boundary of the tool has connected to the negative pole and FI boundary of the electrolyte has an electric potential of 37 V. The temperature condition of the tool (CLMKB) and electrolyte (EJ) surfaces are determined by equations of 4 and 8, respectively.

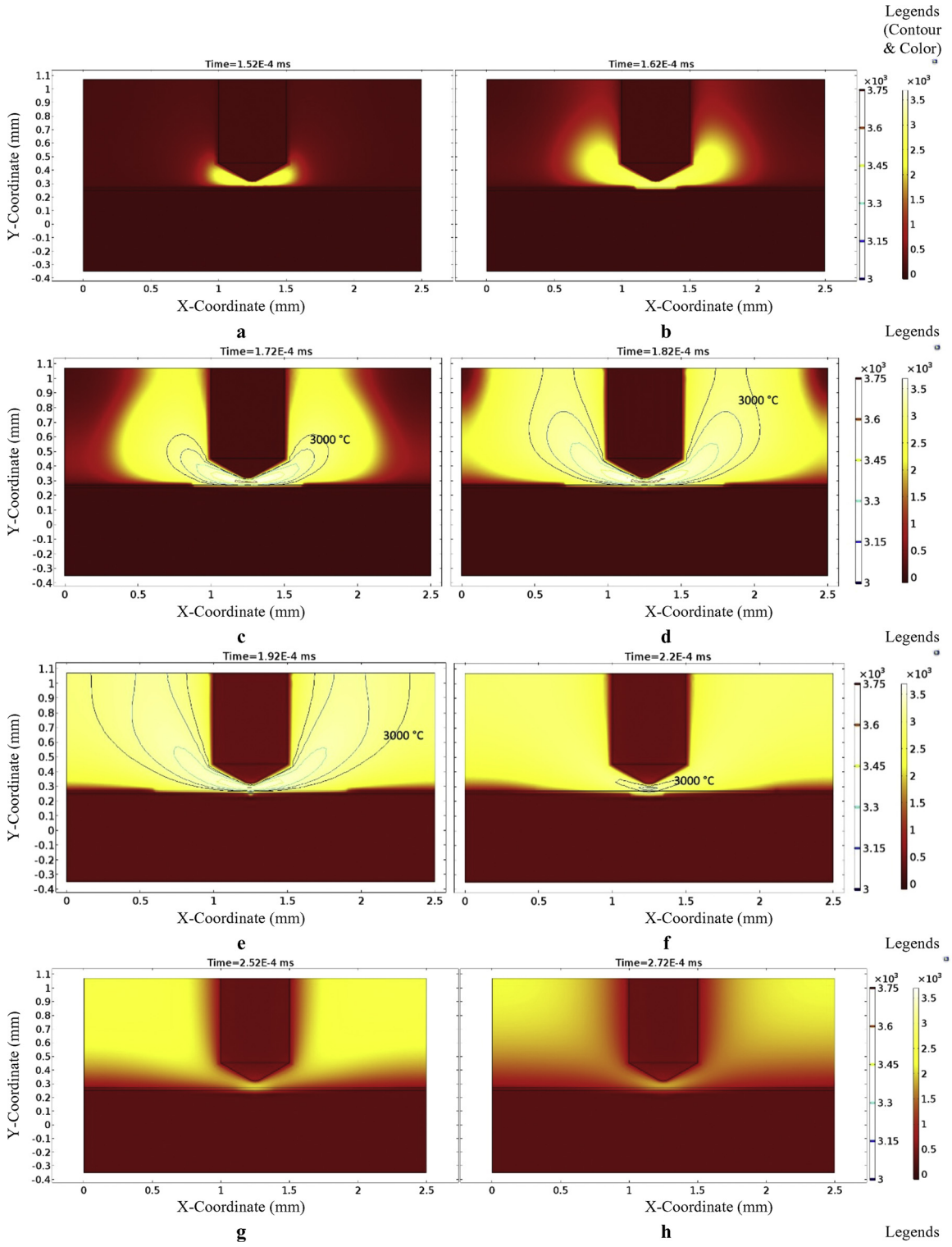

Fig. 6. Consequent images of the temperature distribution and contours (above 3000 ˚C) of discharge phenomenon during the ECDM process a) pulse time:1.52E-4 ms b) pulse time:1.62E-4 ms c) pulse time:1.72E-4 ms d) pulse time:1.82E-4 ms e) pulse time:1.92E-4 ms f) pulse time:2.2E-4 ms g) pulse time:2.52E-4 ms h) pulse time:2.72E-4 ms.

2.5. Results

The main target of this research is an evaluation of MR during the ECDM process. In this regard, two main mechanisms of MR are effective. Between mechanisms, the chemical mechanism has a negligible effect so studying on thermal mechanism can present acceptable data of the total MR. In the first part, the results of temperature distribution for all components besides temperature contours above 3000 ˚C are presented in Fig. 6. As can be seen, the maximum temperature occurs in the hydrogen (positive column) and it is about 3650 ˚C (Fig. 6-d). High-temperature (3000 ˚C) contours start in hydrogen gas from the space between tooltip and the electrolyte layer and expand according to the applied current. The same behavior exists for lower values of temperature contour which extends to the electrolyte and workpiece

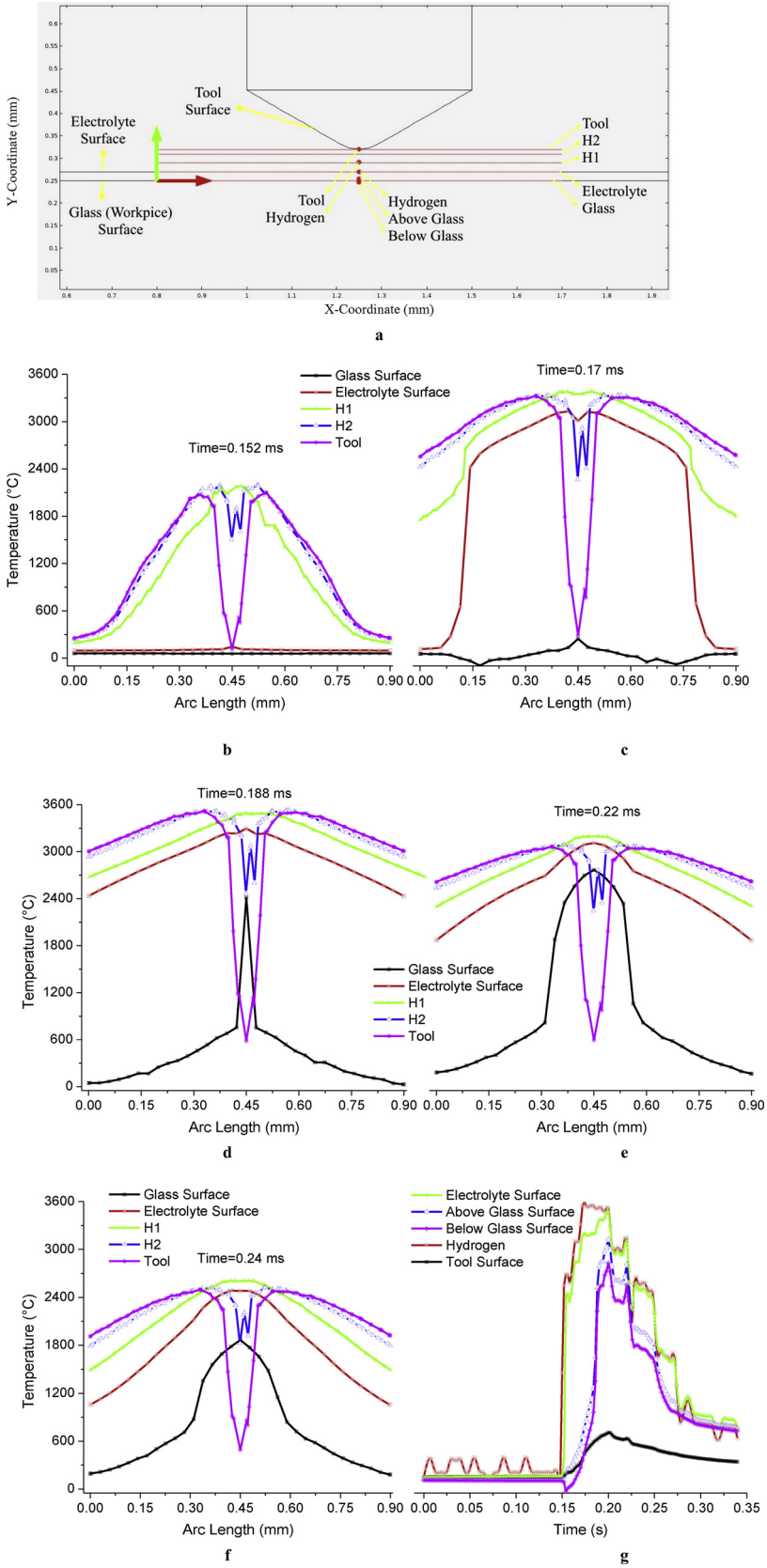

Fig. 7. a) Chosen cut lines and points to study temperature gradients and variations b–f) Temperature results of selected cut lines versus time g) Temperature results of selected points versus time.

Table 1
Thermal conductivity of components.

Component	Temperature range (°C)	Thermal conductivity(W/(m K))
Hydrogen (Plasma Gas)	100–4000	0.3–16.5
Tungsten Carbide (Tool)	100–800	90–70
Soda Lime Glass (Workpiece)	100–1000	0.9–1.4
NaOH Solution (Electrolyte)	100–110	0.663

materials. The specific area of the workpiece reaches the melting point. In continue, the electric current is disconnected and the temperature is reduced in all components.

In order to study details of temperature distribution in the main area of plasma formation (Hydrogen), temperature results along five cut lines (Fig. 7-a) are evaluated and compared in which cut lines are named as the tool, H2, H1, electrolyte, and glass. Fig. 7a,b to f show temperature of cut lines versus time steps of 0.152, 0.17, 0.188, 0.22 and 0.24 ms. Significant temperature gradients are observed during the mentioned time steps. Two main types of variation attract attention in the figures. The local minimum point in the middle of the diagram which is related to cut lines close to the tool. Tool and H2 cut lines have minimum points in the middle of the diagram. The second variation includes H1 cut line temperature versus time. By comparison of Fig. 7c–e, it can be observed that the minimum point in the middle of the diagram in Fig. 7-c is disappeared in Fig. 7-d and replaced with a

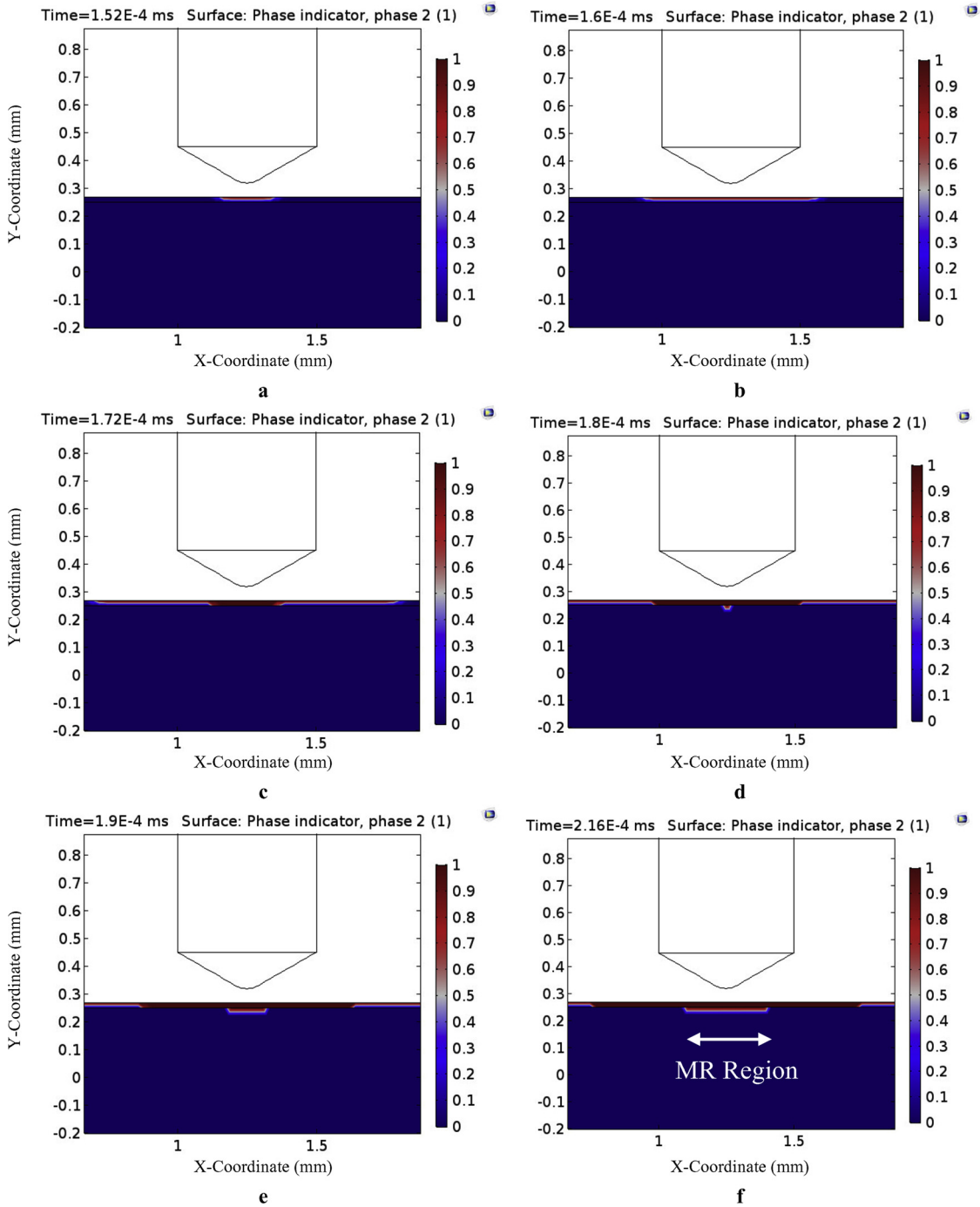

Fig. 8. Consequent images of phase change of electrolyte and workpiece during the ECDM process.

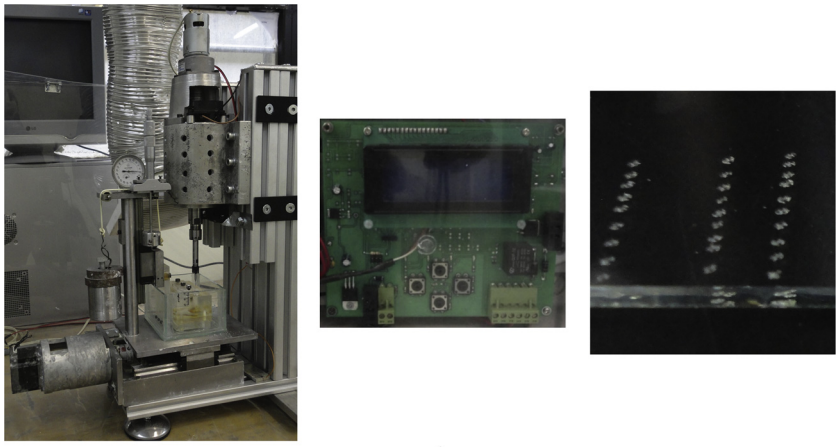

a b c

Fig. 9. a) Experimental configuration b) Electric board (electric pulse generation) c) A sample of fabricated holes on the workpiece [21,22].

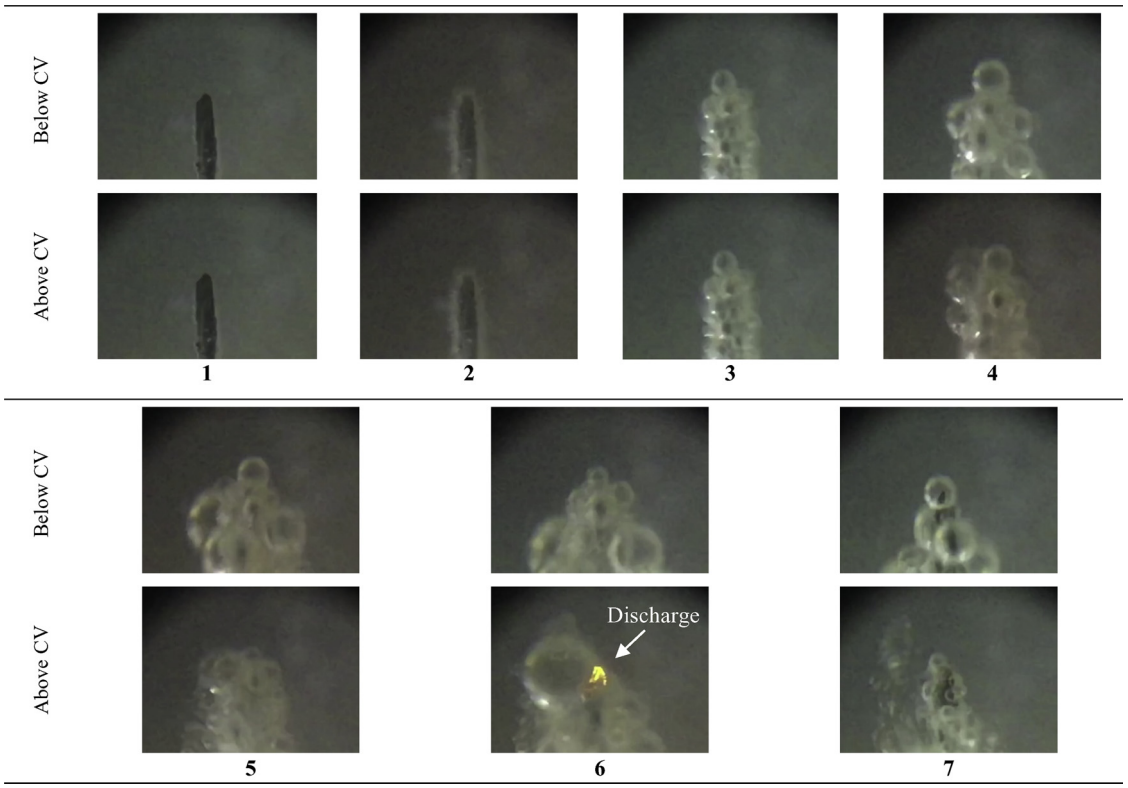

Fig. 10. Consequent images of the tool in two applied voltages slightly below and above the CV. The discharge appears in a voltage slightly above the CV.

maximum point in Fig. 7-e. Both of the mentioned variations can be explained by attention to the thermal conductivity of components. In order to clear understanding, the thermal conductivity of components during practical temperature limits are shown in Table 1. Tool (Tungsten Carbide) has a thermal conductivity several times greater than other components. Hence, regions close to the tool find a lower temperature compared to the neighbor regions in the plasma gas. In the case of H1 cut line, there is a balance condition between heat generation by plasma discharge and heat dissipation through heat conduction of the tool. Comparison of Fig. 7-c and d show that plasma heat generation increases beyond the capacity of heat conduction through the tool so the local minimum point changes to a maximum point. Glass (black) diagram shows the temperature of the workpiece surface which can help to determine the molten material from the workpiece. A comparison of the glass diagram in Fig. 7-d and e show that the maximum width of the diagram happens in Fig. 7-e while the maximum temperature of the system occurs in Fig. 7-e so there is a time delay between maximum values of temperature and MR.

The most critical area in the plasma is the space between the tooltip and workpiece surface so five points are selected to examine temperature variations versus time. Points are selected on the most important sites of the components. Tooltip, electrolyte surface and hydrogen gas are some of the considered points. In order to study the behavior variation from liquid to solid, two points on both sides of the electrolyte-glass interface are considered. As can be seen, the point in the hydrogen experiences the maximum temperature. After the time of 0.2 s, hydrogen and electrolyte temperatures are the same because of electrolyte evaporation and replacement with hydrogen. Tool temperature does not find values more than 800 °C so tool melting does not happen. Oscillations of the diagram mainly originate from the real profile of applied electric current (Section 3.1).

The volume of MR is determined according to the temperature

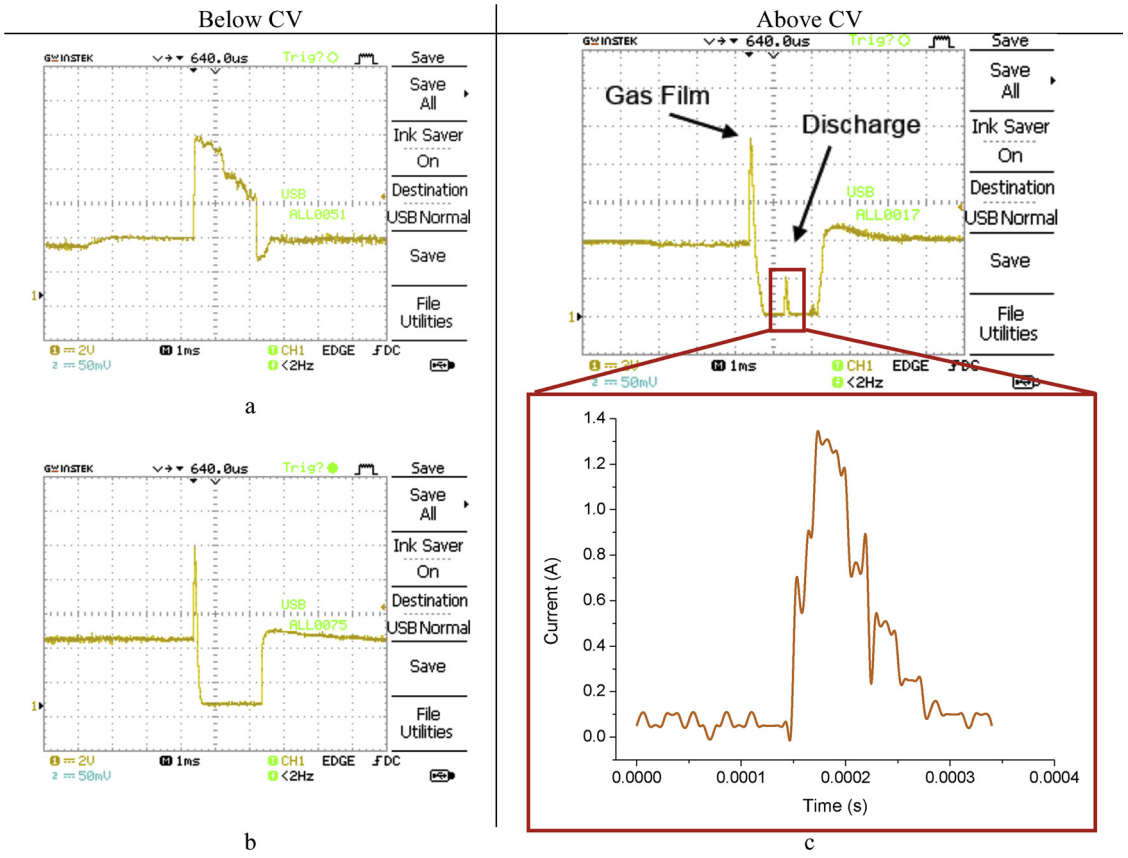

Fig. 11. The current signal diagram in different conditions. In applied voltage lower than CV: a) gas film is not formed b) Gas film is formed without discharge. In applied voltage higher than CV: c) gas film is formed and discharge appears, the profile of consumed electric current considers as the input of simulation.

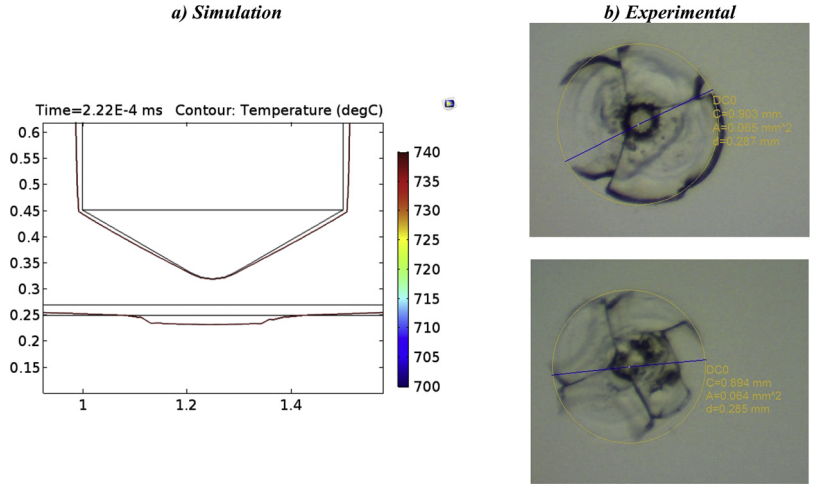

Fig. 12. a) Simulation and b) Experimental results of a single discharge mode of the ECDM process.

distribution and melting temperature of the glass workpiece. In experimental research, Jalali et al. determined 600 ˚C as the melting temperature of glass while they used a gravity feed mechanism in which the tool and workpiece are continuously in contact [18]. Next researchers considered the melting temperature of 600 ˚C for glass workpiece. But in the current research, tool and workpiece are positioned in a constant distance. On the other hand, Jalali et al. studied workpiece temperature during the hydrodynamic regime of machining (machining depth > 300 μm) [18] but in the current research, the discharge regime (machining depth < 300 μm) is applied. In contrast, Elhami et al. considered condition close to the real condition of the ECDM process and stated the temperature of 720 ˚C as the melting temperature (phase change) of the glass workpiece [19]. In the case of the glass workpiece and besides melting temperature, the temperature of phase change of electrolyte is another important factor in the simulations. In a similar condition, Ziki et al. determined the temperature of 110 ˚C as the phase change temperature of electrolyte (NaOH) which is converted from liquid to vapor [20]. In the case of electrolyte phase change from liquid to vapor, transition interval and latent heat were considered as 10 K and 2264 kJ/kg, respectively. Also in case of glass phase change from solid to liquid, transition interval and latent heat were assumed as 20 K and 200 kJ/kg, respectively. Fig. 8 shows the

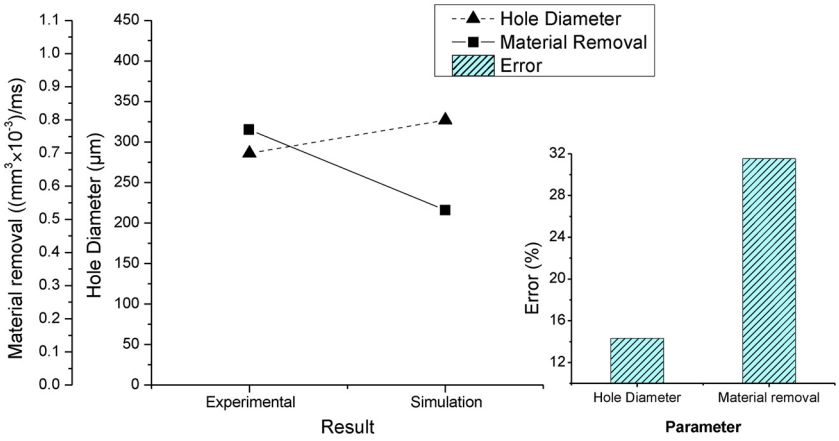

Fig. 13. Comparison of experimental and numerical results and related error values.

phase change boundaries of electrolyte and workpiece versus time. As can be seen, at first, the electrolyte is converted to vapor and in continue, workpiece changes from solid to liquid. Fig. 8 can help to determine the boundary of phase changed material in the workpiece and finally evaluation of the MR. It should be noticed that the effects of vaporized electrolyte and molten workpiece material are not applied in the simulation due to the lack of proper information. Hence, the vaporized electrolyte and melted workpiece are replaced with hydrogen.

3. Experimental verification

3.1. Experimental procedure

The ECDM process in a single discharge mode is applied to verify the simulation results. In this regard, a tool with a conical shape tip and a diameter of 500 μm is fabricated. The tool is positioned at a distance of 70 μm related to the workpiece. The experimental configuration is shown in Fig. 9-a, and includes a gravity feed mechanism to position the tool close to the workpiece with the precision of 1 μm. Also, a special electric board was designed to apply a single electric pulse with adjustable specifications (Fig. 9-b). Electrolyte concentration is considered as 30 %. To measure the MR, every experiment (single discharge mode) is repeated 30 times on the different regions of a workpiece (Fig. 9-c). Finally, using a high precision balance (with the accuracy of 10^{-5} g), total MR is measured and by dividing the number of repetitions, MR caused by a single discharge is determined.

In order to achieve a single discharge, a single electric pulse with a length of 2.1 ms should be applied to the process. Also, the electric voltage is another important parameter which should be adjusted according to Critical Voltage (CV). A CV is a boundary between electrolysis and discharge phenomena. Considering a single electric pulse with a specific length, a voltage higher than CV leads to discharge generation and lower values only result in electrolysis phenomenon and discharge cannot achieve. Fig. 10 shows a series of consecutive images from the ECDM process with voltages slightly above and below the CV. In the present condition, CV is about 37 V which for operational voltage above the CV, a single discharge can be observed and indicated in Fig. 10.

A current signal is an important tool which can show qualitative observation of electrolysis and discharges in a quantitative manner and presents details of the discharge such as discharge power. Two types of the peak can be observed in the current signal diagram which are shown in Fig. 11-c and present formation of gas film and discharge phenomenon. For electric voltage lower than CV, only electrolysis happens in the ECDM process and two states are expected for the gas film. In the first state (Fig. 11-a), the gas film does not form completely and no large peak is expected in the current signal diagram. In the second state (Fig. 11-b), the gas film is formed completely but discharge does not happen. Fig. 11-c shows the condition of the formation of gas film and the happening of single discharge. Current diagram of Fig. 11-c is an indicator of the consumed current during the discharge phenomenon. Electric current was applied as an input into the simulation with a pattern which is extracted from the experiment (Fig. 11-c).

3.2. Results of verification

Simulation results can be verified in two states of hole diameter and volume of removed material (MR). Fig. 12a (simulation) shows the contour of 720 °C in which hole diameter and related MR can be calculated. Fig. 12-b (experimental) shows the experimental results of hole diameter and removed material after applying a single discharge mode of the ECDM process.

A comparison of numerical and experimental results of hole diameter and removed material are shown in Fig. 13. Also, the calculated error between numerical and experimental results are presented by a column diagram. As can be seen, the hole diameter was determined as 286 μm from experiments while simulation predicted a hole diameter of 327 μm. In this case, the numerical model has an error of 14.33 %. According to the removed material (MR), experiments showed a value of 0.771 $(mm^3 \times 10^{-3})$/ms while the numerical model presented the result of 0.528 $(mm^3 \times 10^{-3})$/ms. A comparison of MR results shows the error of 31.5 % for the numerical model to predict experimental results.

Generally, every numerical model associates with some simplifications and assumptions. In this research, some phenomena were ignored during simulation to simplify the running process. In the phase change of electrolyte and workpiece, the effect of electrolyte vapor and workpiece molten material was ignored. The vapor phase of electrolyte improves the ionization of anode and provides more charged particles for plasma propagation. Hence, discharge with more power is expected which enhances the material removal. On the other hand, electrolyte vapor around the plasma column does not effect on the anode ionization but improves heat transfer from the heat affected zone of the workpiece and plasma column. So, side areas of the plasma and close to the hole entrance losses more thermal energy which results in smaller hole diameter.

4. Conclusions

In this research, a new approach was developed to simulate the plasma (discharge) phenomenon during the ECDM process. Despite previous researches, this research implemented a more realistic procedure without the application of Gaussian distribution by considering physical phenomena of discharge such as heat transfer in solid and liquid, electric current, electromagnetic field and coupling of mentioned

phenomena. According to the environmental condition of ECDM discharge, it can be classified as Arc discharge in LTE condition so plasma can be considered as a fluid. The integration of different physics in the outline of the fluid approach of plasma behavior besides the numerical power of COMSOL software were key points to make a new and more realistic model to use in the prediction of ECDM discharge behavior. Results showed that the maximum temperature of 3650 °C is possible in the positive column of plasma. Temperature distribution showed that regions close to the tool found a lower temperature compared to the workpiece neighbor regions. Phase change results clearly determined the volume of workpiece material which was molten and removed from the workpiece surface. Consecutive actual images and related current signal diagrams were recorded to determine the critical voltage which is 37 V in applied condition. The numerical model presented the MR value of 0.528 ($mm^3 \times 10^{-3}$)/ms in specific conditions while in the same state, experiments resulted in the MR value of 0.771 ($mm^3 \times 10^{-3}$)/ms. Mentioned data showed that the developed model had an error of 31.5 % in the prediction of MR during the ECDM process. In the case of hole diameter, as the second important output, the developed model predicted more accurate results with an error of 14.33 %.

Declaration of Competing Interest

The authors declare that they have no known competing financial interests or personal relationships that could have appeared to influence the work reported in this paper.

The authors declare the following financial interests/personal relationships which may be considered as potential competing interests.

Acknowledgment

The authors would like to appreciate Iran National Science Foundation (INSF) to support this research plan.

References

[1] Sarkar B, Doloi B, Bhattacharyya B. Electrochemical discharge micro-machining of engineering materials. Non-traditional micromachining processes. Springer; 2017. p. 367–92.
[2] Francis FC. Introduction to plasma physics and controlled fusion. Plasma Phys 2015.
[3] Wuthrich R, Ziki JDA. Micromachining using electrochemical discharge phenomenon: fundamentals and application of spark assisted chemical engraving. William Andrew; 2014.
[4] Fridman A. Plasma chemistry. Cambridge university press; 2008.
[5] Max FH. Arc physics. New York: Springer-Verlag; 1968.
[6] Jain V, Dixit P, Pandey P. On the analysis of the electrochemical spark machining process. Int J Mach Tools Manuf 1999;39:165–86.
[7] Bhondwe K, Yadava V, Kathiresan G. Finite element prediction of material removal rate due to electro-chemical spark machining. Int J Mach Tools Manuf 2006;46:1699–706.
[8] Wei C, Xu K, Ni J, Brzezinski AJ, Hu D. A finite element based model for electrochemical discharge machining in discharge regime. Int J Adv Manuf Technol 2011;54:987–95.
[9] Jiang B, Lan S, Ni J, Zhang Z. Experimental investigation of spark generation in electrochemical discharge machining of non-conducting materials. J Mater Process Technol 2014;214:892–8.
[10] Jiang B, Lan S, Wilt K, Ni J. Modeling and experimental investigation of gas film in micro-electrochemical discharge machining process. Int J Mach Tools Manuf 2015;90:8–15.
[11] Kamaraj AB, Jui SK, Cai Z, Sundaram MM. A mathematical model to predict overcut during electrochemical discharge machining. Int J Adv Manuf Technol 2015;81:685–91.
[12] Goud M, Sharma AK. A three-dimensional finite element simulation approach to analyze material removal in electrochemical discharge machining. Proceedings of the Institution of Mechanical Engineers, Part C: Journal of Mechanical Engineering Science 2016. 0954406216636167.
[13] Yos JM. Transport properties of nitrogen, hydrogen, oxygen, and air to 30,000 K. DTIC document. 1963.
[14] Comsol A. Comsol documentation, comsol multiphysics users guide. 2005.
[15] Kellogg HH. Anode effect in aqueous electrolysis. J Electrochem Soc 1950;97:133–42.
[16] Garbarz-Olivier J, Guilpin C. The origin of the electrode effect in various electrolytes. J Electroanal Chem Interfacial Electrochem 1978;91:79–91.
[17] Heath M, Woodfield PL, Hall W, Monde M. An experimental investigation of convection heat transfer during filling of a composite-fibre pressure vessel at low Reynolds number. Exp Therm Fluid Sci 2014;54:151–7.
[18] Jalali M, Maillard P, Wüthrich R. Toward a better understanding of glass gravity-feed micro-hole drilling with electrochemical discharges. J Micromech Microeng 2009;19. 045001.
[19] Elhami S, Razfar M. Analytical and experimental study on the integration of ultrasonically vibrated tool into the micro electro-chemical discharge drilling. Precis Eng 2016.
[20] Ziki JDA, Hof LA, Wüthrich R. The machining temperature during spark assisted chemical engraving of glass. Manuf Lett 2015;3:9–13.
[21] Elhami S, Razfar M. Effect of ultrasonic vibration on the single discharge of electrochemical discharge machining. Mater Manuf Process 2018;33:444–51.
[22] Elhami S, Razfar M. Study of the current signal and material removal during ultrasonic-assisted electrochemical discharge machining. Int J Adv Manuf Technol 2017;92:1591–9.